ELSEVIER

Contents lists available at ScienceDirect

Estuarine, Coastal and Shelf Science

journal homepage: www.elsevier.com/locate/ecss





Drifter and dye tracks reveal dispersal processes that can affect phytoplankton distributions in shallow estuarine environments

Natalie L. Geyer^a, Dhruv Balwada^b, Elizabeth Simons^c, Kevin Speer^{c,e}, Markus Huettel^{d,*}

- a Department of Earth, Ocean and Atmospheric Science, Florida State University, Tallahassee, FL, 32306, USA
- ^b School of Oceanography, University of Washington, Seattle, WA, 98195, USA
- ^c Geophysical Fluid Dynamics Institute, Florida State University, Tallahassee, FL, 32306, USA
- d Department of Earth, Ocean and Atmospheric Science, Florida State University, 1011 Academic Way, Tallahassee, FL, 32306-4520, USA
- e Department of Scientific Computing, Florida State University, Tallahassee, FL, 32306, USA

ARTICLE INFO

Keywords: Phytoplankton patchiness Density front Dye tracer Drifter Estuarine mixing

ABSTRACT

In shallow estuarine environments, the time scales of hydrodynamic processes that control particle distribution may outpace the time scales of phytoplankton patch formation through reproduction. Consequently, physical processes can dominate the distribution of the phytoplankton, but these processes and their dynamics are not well understood. Here we used flow measurements with a bottom mounted Acoustic Doppler Current Profiler (ADCP), shipboard hydrographic transects, drifter releases, and Rhodamine dye to characterize the small-scale flow environment and its effect on dispersion processes in a shallow estuarine environment, Apalachicola Bay, Florida. Spatial spectra of salinity and chlorophyll followed a power law behavior of -3 at length scales of 250 m-5 km. The ADCP data revealed the presence of a vertically sheared flow that was strongly modulated by tides and bottom topography. Tidal flows had a characteristic magnitude of 20-40 cm s⁻¹, with durations of flow reversals between the near-surface and bottom flows. Drifter triplets indicated shear and strain rates on the order of $10^{-3} - 10^{-4}$ s⁻¹, and single particle dispersion rates (diffusivity) of 0.1 m² s⁻¹. The area evolution of the dye patch observed by a drone corresponded to eddy diffusivity comparable to those estimated from drifters, or about 0.1 m² s⁻¹. The dye patch experiments demonstrate how physical processes at scales of 1–100 m can affect the shape and development of phytoplankton patches in the bay. Vertical shear, produced by wind directions deviating from flow direction, can broaden and divide a plankton patch by transporting different depths of a patch in different directions. When winds and currents are aligned, shear leads to elongation and narrowing of the patch. The results indicate that the small-scale flow environment in estuaries can be pivotal in controlling the distribution and dispersal of planktonic organisms and thereby becomes a decisive factor for the development and breakdown of phytoplankton communities.

1. Introduction

When favorable conditions promote growth of a phytoplankton organism, rapid reproduction ensues leading to the local accumulation of cells, a phytoplankton patch, and to first order phytoplankton cells can be considered passive particles. Hydrodynamics, grazing and plankton behavior then may control the spatial and temporal development of the phytoplankton patch. Phytoplankton organisms therefore are not distributed uniformly, and individuals occur more frequently together than predicted from a random distribution. Satellite images reveal large-scale patterns of phytoplankton distribution, and the light emission

spectrum of chlorophyll can be used for estimates of phytoplankton abundance and biomass. Although small amounts of free chlorophyll released by decaying plant material may occur in the water column, chlorophyll concentration is a useful and widely accepted proxy for phytoplankton and its patchy distribution (Behrenfeld et al., 2005; Behrenfeld and Falkowski, 1997; Jimenez et al., 1987; Longhurst, 1995). Owing to its spatial and temporal dynamics, describing phytoplankton patchiness is complex, and typical methods include Fourier power spectra analysis, multi-point correlation functions, wavelet analysis, and multifractal analysis. Because the spatial heterogeneity influences productivity, diversity, and foodweb stability, understanding the controls of

E-mail addresses: nataliebyars@gmail.com (N.L. Geyer), dbalwada@ldeo.columbia.edu (D. Balwada), elizabeth.g.simons@gmail.com (E. Simons), kspeer@fsu.edu (K. Speer), mhuettel@fsu.edu (M. Huettel).

^{*} Corresponding author.

phytoplankton patchiness is prerequisite for assessing the functioning of the marine ecosystem (Martin, 2003).

Phytoplankton communities are dispersed by water currents and associated turbulence (Mackas et al., 1985; Okubo, 1978; Prairie et al., 2011). Characterizing the fluid flow and its variability therefore is essential for developing models of phytoplankton distribution and ecology. Spatial heterogeneity of environmental factors, such as current velocities, salinity, nutrients, light, and grazers, modulate the patchy distribution of phytoplankton (Harris, 1986; Haury et al., 1978), which has implications for the productivity and trophodynamics of an ecosystem (Martin, 2005; Roman et al., 2005; Wetz et al., 2011). Most studies characterizing phytoplankton patchiness and the processes influencing it have been conducted in the coastal and open oceans (Mahadevan, 2016; Martin, 2003); and phytoplankton patchiness in estuarine environments thus has remained poorly understood.

A characterizing feature of most estuaries is that they are relatively shallow, typically with average water depth of less than 10 m (Bricker et al., 2008), which sets their hydrodynamics and controls of phytoplankton distribution apart from those of deeper marine systems. Factors controlling patchiness in estuaries that differ from those in the open ocean include river discharge, steep density and nutrient gradients, local winds, and the morphology of the estuary (Dustan and Pinckney, 1989; Lucas et al., 1999; Mortazavi et al., 2000; Roman et al., 2005). The dominant temporal scales of estuarine processes/mixing also tend to be shorter than those in the open ocean because of the smaller spatial scales (including water depth) and strong tidal influences (Fischer, 1976; Geyer and Signell, 1992). In Apalachicola Bay/Florida, Geyer et al. (2018) observed small-scale patches of phytoplankton with widths of 0.1-4.5 km and steep chlorophyll a (Chl a) gradients. These small patches, which often were associated with density fronts, accounted for about 10% of the phytoplankton biomass along the sampled transects and thus were significant. However, the mechanisms shaping these patches were not clear.

The present lack of understanding of the processes controlling this patchiness limits the ecological conclusions that can be drawn from these observations and ultimately quantification of estuarine phytoplankton. This lack is significant as estuaries are among the most productive environments in the oceans (Boynton et al., 1982; Cloern et al., 2014), are of exceptional ecological and economical importance (Bundy, 1992; Day et al., 2012; Mansur et al., 2016), and now are disproportionally threatened by climate change, sea level rise, nutrient input and other human activities (Camargo and Alonso, 2006; Rabalais et al., 2009; Rabouille et al., 2001).

To address this lack in understanding, we initiated a study designed to characterize and assess physical processes that contribute to the controls of small-scale estuarine phytoplankton distribution patterns as those observed in Apalachicola Bay estuary in August 2011 (Geyer et al., 2018). Our process study uses flow tracer and drifter deployments as well as current measurements to assess the influence of estuarine flow characteristics on transport and dispersion of mock-phytoplankton patches represented by inert dye tracer patches. Main goals were to quantify lateral advection and dispersion processes on short timescales (minutes to hours) in the dynamic surface layer (<1 m), and to compare the purely physically controlled distribution characteristics of tracer dye patches with distribution characteristics of phytoplankton patches we observed in the same estuary in 2011. This comparison suggests that small scale physical flow and mixing processes can dominate phytoplankton distributions in estuarine settings, and underscores the combination of synoptic high-resolution physical, biological, and chemical measurements required for untangling the controls of phytoplankton bloom evolution in these productive key environments.

2. Methods

The in-situ work in Apalachicola Bay/Florida utilized Lagrangian drifters, aerial drone photography, boat-mounted flow-through sensors,

and fixed current meters to investigate the transport of the mockphytoplankton patches (i.e., dye) and the adjacent waters. Lagrangian drifter data (Davis, 1991) allow an improved determination of diffusion coefficients (Pal et al., 1998) that affect the distribution of phytoplankton, nutrients, or pollutants. Likewise, passive dye tracers are a powerful tool for studying transport and circulation patterns in the open and coastal ocean (Garrett, 1983; Sundermeyer and Ledwell, 2001; Sundermeyer et al., 2005; Watson and Ledwell, 2000; Yu et al., 2016), estuaries (Bailey, 1966; Chant et al., 2007), and near-shore environment (Brouwer et al., 2016; Clark et al., 2014). Fluorescent dyes stain the water and allow the movement of the water (and thereby substances within, such as plankton, nutrients, or pollutants) to be traced visually or with fluorometers. Since the dye is a practically inert tracer, dye patches offer insight into the non-biological drivers of patch development. The recent developments of remotely controlled drones with onboard cameras facilitates inexpensive aerial observation of the dye tracer movement (Brouwer et al., 2016; Tauro, 2016).

2.1. Study site

The in-situ study was conducted over 4 days, from March 30 - April 2, 2015, in the western region of Apalachicola Bay (AB), a bar-built, microtidal estuary located in the Northeastern Gulf of Mexico (Fig. 1). The estuary has an east-west length of 63 km, and a north-south width of 12 km at its widest points, with an average depth of 2-3 m (Edmiston, 2008). The bay receives freshwater from the Apalachicola River, the largest river in Florida by flow volume, and opens to the ocean through four inlets: East Pass, Sikes Cut, West Pass, and Indian Pass. Aside from intermittent strong winds, the energetic currents in the bay are driven to first order by differences in tidal amplitudes between these different passes, with most of the inflow being through East Pass. Local reversals can be seen in the western region when the flood tide pushes water in through the western passes (Huang et al., 2002b). Sustained along-estuary winds can modulate and even reverse the tidal surface currents (Huang and Foo, 2002; Huang et al., 2002a). Long-term average annual wind velocity is 3.5 ± 0.4 m s⁻¹, with the main direction November-June from the east, turning more north during July to October. Mean tidal range in AB is 65 \pm 16 cm. In 2015, the average water temperature in the center of the bay (Cat Point) was 23.4 $^{\circ}\text{C}$ (range: 9.7–33.7 °C), salinity 22.3 \pm 6.5 (3.4–33.9) and river discharge $573 \pm 579 \ m^3 \ s^{-1}$ (178–5040 $m^3 \ s^{-1}$). This discharge creates a residual flow controlling flushing times of the bay, which ranges from 6 to 12 days (Dulaiova and Burnett, 2008; Morey and Dukhovskoy, 2012). For more detailed descriptions of the system with respect to its temperature, salinity and flow dynamics the reader is referred to (Huang et al., 2002a, 2002b; Huang and Foo, 2002; Morey and Dukhovskoy, 2012).

2.1.1. Environmental characteristics at the study site: winds, tidal amplitudes and river discharge

Local wind velocity (5 s data averaged over 15 min intervals) and water level data were collected by the Apalachicola National Estuarine Research Reserve at the Dry Bar monitoring station (Fig. 1a). The wind gage was located 10 m above the water surface. During the study, winds primarily blew from the west on the first 3 days, gradually increasing in strength before weakening and shifting to blow from the south and southeast on Day 4 (Fig. 1b).

Tides were followed through monitoring water depth, measured by a YSI 6600 EDS multiparameter sonde affixed to the piling 0.3 m from the sediment surface in approximately 2 m of water. The tides were mixed on the first day, gradually trending towards a more semi-diurnal characteristic towards the end of the experiment (Fig. 1b).

Daily river discharge was retrieved from the USGS river gage (02359170) at Sumatra, Florida (http://waterdata.usgs.gov/nwis/dv), 33 km upstream from the Apalachicola River mouth. During the course of the experiment, river discharge was 635 ± 12 m³ s⁻¹, which, according to Dulaiova and Burnett (2008), results in a flushing rate of

(a)

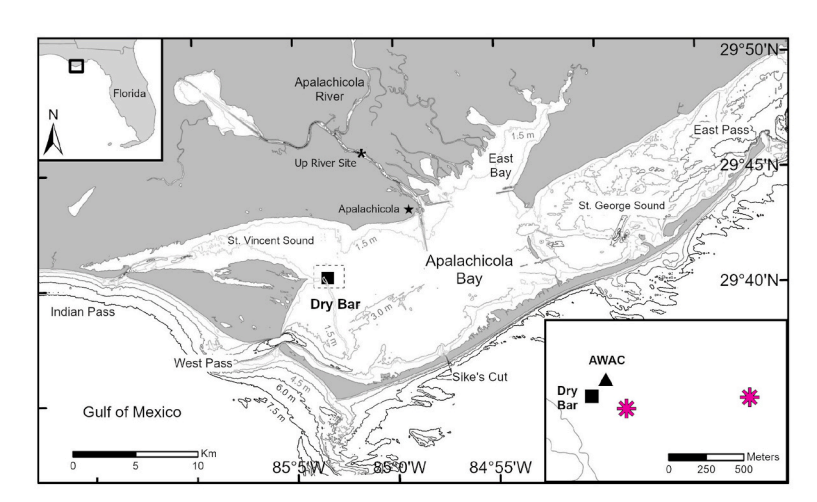
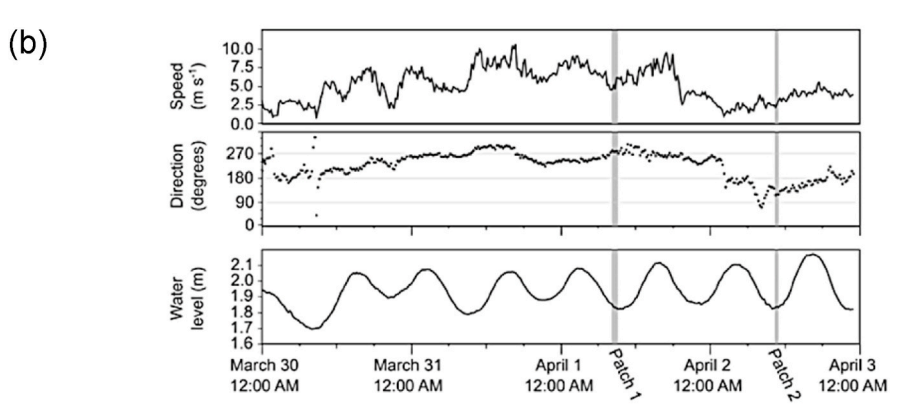


Fig. 1. (a) Study site in Apalachicola Bay, Florida, and its location in the Northeastern Gulf of Mexico (inset top left). Inset (bottom right) details the dashed square labeled Dry Bar in the main figure and depicts the relative locations of the Dry Bar piling (solid square), AWAC (solid triangle) and dye release sites (pink asterisks). (b) Wind speed and direction (180° indicates wind from the south), and water level at Dry Bar. Gray bars indicate times of dye experiments. (c) Satellite image showing the uneven distribution of phytoplankton and suspended matter in the bay (image: NASA). (For interpretation of the references to color in this figure legend, the reader is referred to the Web version of this article.)





approximately 10 days. River discharge and inflow of Gulf water into the bay during flood generate a complex flow environment (Fig. 1c) as well as strong salinity gradients and stratification in AB. Stratification during the study period was primarily controlled by salinity and varied significantly based on location and tidal cycle. A 3-year study conducted in AB by Mortenson (2013) revealed temperature variations with depth $< 1\,^{\circ}\mathrm{C}$ confirming vertical density variation dominated by salinity differences.

2.2. Analyses of previous data to assess small-scale spatial structure of physical and biological tracers in AB

To demonstrate how physical processes may contribute to the controls of small-scale estuarine phytoplankton distribution patterns in estuarine settings, we compare the observed dye distribution patterns caused by physical processes to distribution patterns observed in natural

phytoplankton distributions. The latter were extracted from data we collected in AB in 2011 (Geyer et al., 2018). A direct causal link between physical processes and phytoplankton distribution may only be established through simultaneous measurements of these processes and associated distributions. We therefore emphasize that while our comparison between dye patch evolution measured in 2015 and phytoplankton patches observed in 2011 can provide indications of the influence of physical factors affecting estuarine phytoplankton distribution, the 2015 numerical results cannot be applied directly to the 2011 AB observations as the time periods of physical and biological measurements differ.

In the 2011 measurements, the horizontal distributions of salinity and Chl a were recorded at scales of 10's to 1000's meters (0.5 m below surface, 5 s intervals) using a flow-through profiling instrument (Data-Flow, Madden and Day, 1992). The georeferenced data had a spatial

resolution of approximately 50 m. We analyzed the power spectra of salinity and Chl a of five of these transects that each had a length of approximately 23 km and were sampled over a period of approximately 30-45 min, each (Fig. 2a and b). The tracers measured along the transects first were linearly interpolated to a uniform grid with 50 m spacing, then a slowly varying mean, which was estimated using a moving average with a 3 km window, was removed from the data to minimize the influence of a slowly varying background signal (Franks, 2005) or tidal aliasing. Slowly varying background signals were caused by tidal movements and river outflow, which can be seen as anomalously fresh signals in some of the salinity transects (Fig. 2b). The power spectra were estimated using the high-pass data, after the slowly varying mean had been removed, and a multi-taper spectral estimation technique. These spectra are representative of the spectral characteristics of features smaller than about 3 km in size, which is the scale where we anticipate the largest signatures of the tracer stirring. We used the mspec function in the jSpectral module of the jLab package (http://www.jmlill v.net/doc/jLab.html) for the spectral calculations.

2.3. Observational platforms, data processing, and analysis techniques

2.3.1. Flow measurements by AWAC, Eulerian frequency spectra

An Acoustic Current Profiler (Nortek AWAC) was moored for 50 h (Days 2–4; March 31 – April 2, 2015) about 150 m northeast of the Dry Bar Station (29°40.48′ N, 85°03.50′ W) in 3 m of water (Fig. 1). The AWAC recorded current velocities once every 5 min with a bin height of 0.5 m, providing 4 velocity measurements in a vertical profile between depths of 0.5–2.5 m. The deepest bin was about 0.5 m above the sediment. The number of samples per burst was 1024 sampled at 4 Hz.

The power spectrum, in frequency domain, was calculated using the same methods as those used for calculating wavenumber spectra of tracers. In contrast to the spatial spectrum, this analysis characterizes the variability of the flows over different time periods. For the velocity, a constant time mean and linear trend were subtracted before calculating

the spectrum. In addition, we calculated a running average with half window length of 30 min (using the "nanmoving_average" function in Matlab) to present the slowly varying part of the flow.

2.3.2. Drifters, flow kinematics, and single particle diffusivities

Three Davis-style drifters (Lumpkin et al., 2017) were deployed and recovered during the flood tide (~08:00 to 13:00 EST) each day at the locations shown in Fig. 4. The drifters were 0.5 m wide and reached 0.5 m deep into the water, allowing them to be advected with the top layer of the water column with minimal wind drag. All three drifters were outfitted with a NOAA TrackPack (https://comet.nefsc.noaa.gov/ioos/drift/driftdesign.html#General_Mission) that was set to transmit its GPS coordinates every half hour via satellite communications.

Two Garmin DC40 units (3 s refresh rate) were also used to augment the temporal resolution of GPS tracks of two drifters and gather higher temporal resolution data. However, we were unable to recover complete trajectories from drifters due to an error in device setup, thus the higher resolution data from these units were only available for part of the drifter deployment.

Kinematic properties of the horizontal flow – shear, strain, divergence and vorticity – were estimated using the technique described in Molinari and Kirwan Jr (1975). This method assumes that locally the flow can be described as a mean flow and contributions from linear gradients in velocities (first two terms in a Taylor series). The mean flow is estimated using the mean drift of a cluster of drifters, and the gradients are estimated using a least-squares fit to the differences in velocities of the different drifters. These velocity gradient estimates inform the different kinematic measures of the flow. This method requires simultaneous measurements from at least 3 drifters, and we used the drifter positions from the TrackPacks for these estimates. Further details of this calculation are presented in the Supplementary Material A.

The velocity gradients that stretch fluid parcels apart are also indicative of the processes active in dispersing the fluid. A measure of

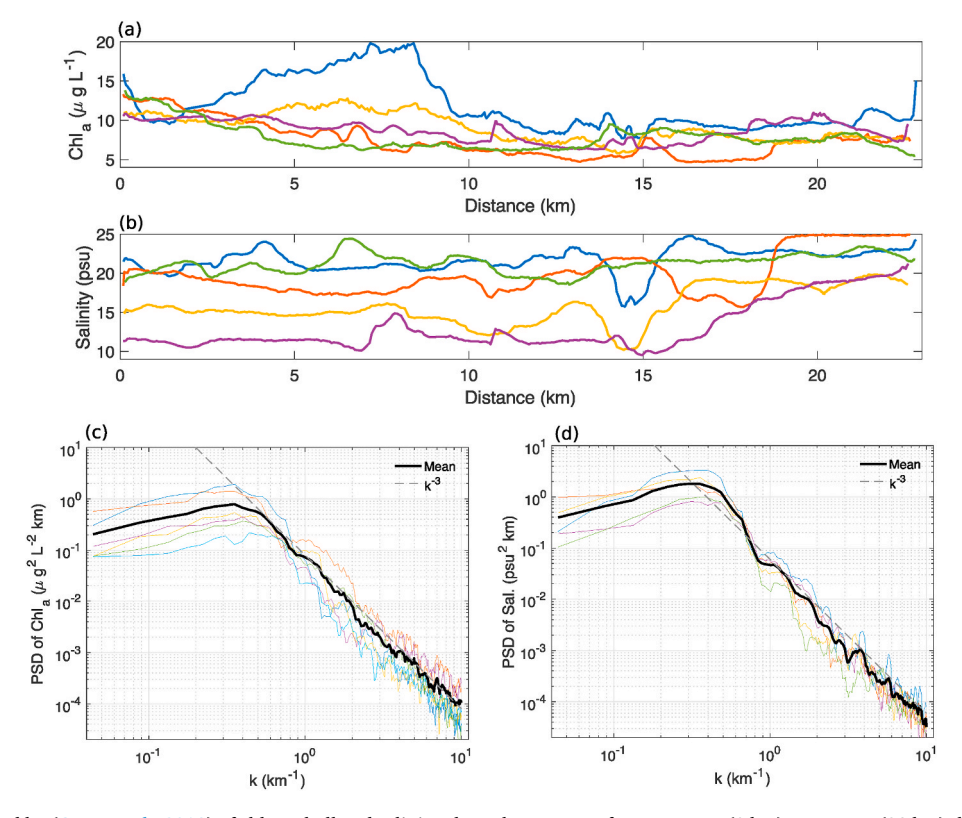


Fig. 2. (a, b) Data recorded by (Geyer et al., 2018) of chlorophyll and salinity along the transects from East Bay (0 km) to Dry Bar (23 km) that were analyzed for this study. (c, d) Spectra of Chl a and salinity; thin colored lines are the power spectra from individual transects and thick black line is an average.

the rate of stretching, the longitudinal second order velocity structure functions $(S2_l)$, can be calculated from pairs of drifters and quantifies the magnitudes of the stretching velocity as a function of the distance between the fluid parcels (Babiano et al., 1990).

$$S2_l(r) = \langle \delta u_l(r)^2 \rangle$$

Where <.> indicates averaging over all pairs of drifters that are within a separation distance, r, from each other. δu_l is the longitudinal velocity difference, where longitudinal is in the direction of the axis joining the two drifters.

Single particle diffusivities were estimated using the method outlined in Suara et al. (2016) following the techniques from Davis (1991). The velocity from a single drifter is decomposed into the large-scale flow component (which can be a spatial or temporal mean) and the residual eddy flow (which is the component whose effects are meant to be represented by an eddy diffusivity). The residual eddy velocity time series are used to calculate the characteristic eddy energy - velocity variance (u'²), and a Lagrangian time scale (T_L) from the lagged autocorrelation. The eddy diffusivity is defined as $K = (u^2) T_L$. Further details of the diffusivity calculation and sensitivity to definition of mean flow and drifter position processing are presented in the Supplementary Material T_L

2.3.3. Dye experiments

A neutrally buoyant solution of Rhodamine WT (RWT) was released and monitored with aerial photography to visualize a simulated phytoplankton patch. RWT is a bright pink dye commonly employed to trace and visualize physical transport in water on short spatiotemporal scales (Bogucki et al., 2005; Clark et al., 2014; Mirfenderesk et al., 2007). This fluorescent dye was chosen because of its relatively low toxicity, favorable chromatic properties, low particle affinity and slow photolysis rates (Smart and Laidlaw, 1977; Suijlen and Buyse, 1994). To keep the dye in the surface layer that had a density of 1.007-1.019 g cm⁻³, dry RWT dye powder (39% RWT by weight) was mixed with fresh water at a ratio of 3 g L⁻¹ to yield a solution with a density of 1.003 g cm⁻³. Two dye release experiments were conducted on Days 3 and 4. Each experiment was initiated by partially submerging a bucket of dye solution to allow the dye to enter the surface water with minimal mixing during the release. A total of 68 L dye solution was deployed with 4 buckets within ~2 min. Two drifters were released concurrently with the dye solution; one at the beginning of the release and one after all the dve was deployed.

A DJI Phantom 2 Vision + drone captured aerial photographs of the spreading dye patch beginning at 1--6 min after completion of the dye releases, and then at 30-s time intervals. The 14 megapixel camera was angled downward to zero degrees and recorded images in RAW format. Drone flight software provided altitude data, and the onboard GPS allowed the drone to maintain its position with a 0.8 m vertical and 2.5 m horizontal hover accuracy (DJI, 2017). All images were stamped with a center point GPS location in WGS84 datum (error \pm 3 m). Aerial imagery was pre-processed in Adobe Lightroom and ImageJ, then georeferenced in ArcGIS (details of processing are in Supplementary Material C).

The scaling of the drone camera photographs was calibrated using images of markers spaced at known distances. The drifters were visible in the dye patch pictures, providing an in-situ spatial calibration reference.

Dye traveling distances were measured using the displacement of the visually distinct leading edge of the dye patch in consecutive pictures. Lateral advection velocity of the dye patch was calculated by dividing dye travel distance by the length of the time interval between pictures. The mean advection calculated with this method agreed with the mean advection calculated using the approximate centroid of the dye patch.

During the dye experiments, salinity at $0.5\ m$ depth was measured with the Dataflow flow-through instrument. The boat speed during the

measurements was $\sim\!3.5$ km h^{-1} and the transect lengths across the dye patch were 200–400 m long producing data with a spatial resolution of approximately 5 m. The analysis of the georeferenced data was completed in ArcGIS. In addition, vertical salinity profiles were conducted with a YSI 6600 Sonde.

3. Results

In this section, we first present results from the analysis of the data reported by Geyer et al. (2018) with focus on salinity and Chl α small-scale spatial distributions in AB. We then explain current characteristics revealed by the AWAC measurements before addressing the results of the Lagrangian experiments. These drifter and dye experiments reveal details of the small-scale processes that influence the development of patchiness.

3.1. Characteristics of spatial salinity and Chl a distribution based on data reported by Geyer et al. (2018)

The measurements of physical, chemical, and biological variables collected along repeat transects in the bay by Geyer et al. (2018) revealed distinctive spatial and temporal variability of these variables. Here we present a wave-number (1/wave-length), or inverse length-scale based characterization of the spatial variability of salinity and chlorophyll along the longest repeat transect, which extended from East Bay to Dry Bar (0 km–23 km, respectively, in Fig. 2a–b).

Both salinity and Chl a have a large scale structure defined by the fresher and more chlorophyll rich water in East Bay (Geyer et al., 2018). The small scale variability of this large scale structure can be characterized through a wavenumber power spectrum (Fig. 2c–d), which here follows a power law behavior, with an exponent of -3, at scales of 0.1–3 km. The slight elevation in the salinity spectrum above the power law behavior, at scales around 2–3 km, is caused by the presence of the freshwater river plume in the transects.

Stirring by the flow in the estuary cascades tracer variance from large scales to small scales, breaking large filaments into smaller filaments. At the smallest scales, these tracer variances are removed by molecular diffusion. Simple models of turbulent flows, which assume homogeneity, isotropy, and statistical stationarity, predict the tracer variance to have power law behavior with slopes in the log-log plot (exponent of the power law), between -2 and -1. Steeper tracer spectrum slopes are indicative of the flow having more kinetic energy at smaller scales, which is reflected in a flatter kinetic energy spectrum encompassing higher wavenumbers before dropping off. The spectral slope of -3 is relatively steep, suggesting that flows at small scales in the bay are energetic. In an inhomogeneous Bay environment, mean flows with complex spatial structures may result from the presence of bottom topography at small scales and complex lateral coastal boundaries, with localized tracer sources and sinks.

Simple models that rely on homogeneity, isotropy, and smoothly varying background tracer structures, therefore, might not be applicable in AB. Nevertheless, spectral behaviors of salinity (passive tracer) and Chl *a* (reactive tracer) collected along the repeat transects in the bay by Geyer et al. (2018) were very similar, suggesting that at these length scales the dominant controls structuring tracer distributions were physical.

3.2. Currents

The AWAC data provided information about the general properties of the currents at the study site (Fig. 3a–b). The time series underline the strong imprint of the tidal modulation, with a typical amplitude around 30 cm s $^{-1}$. There was substantial vertical shear in the flow, with numerous instances when the near surface and near bottom flows moved in opposite direction.

During the tracer experiment, the flow at 1.5 m above the bottom

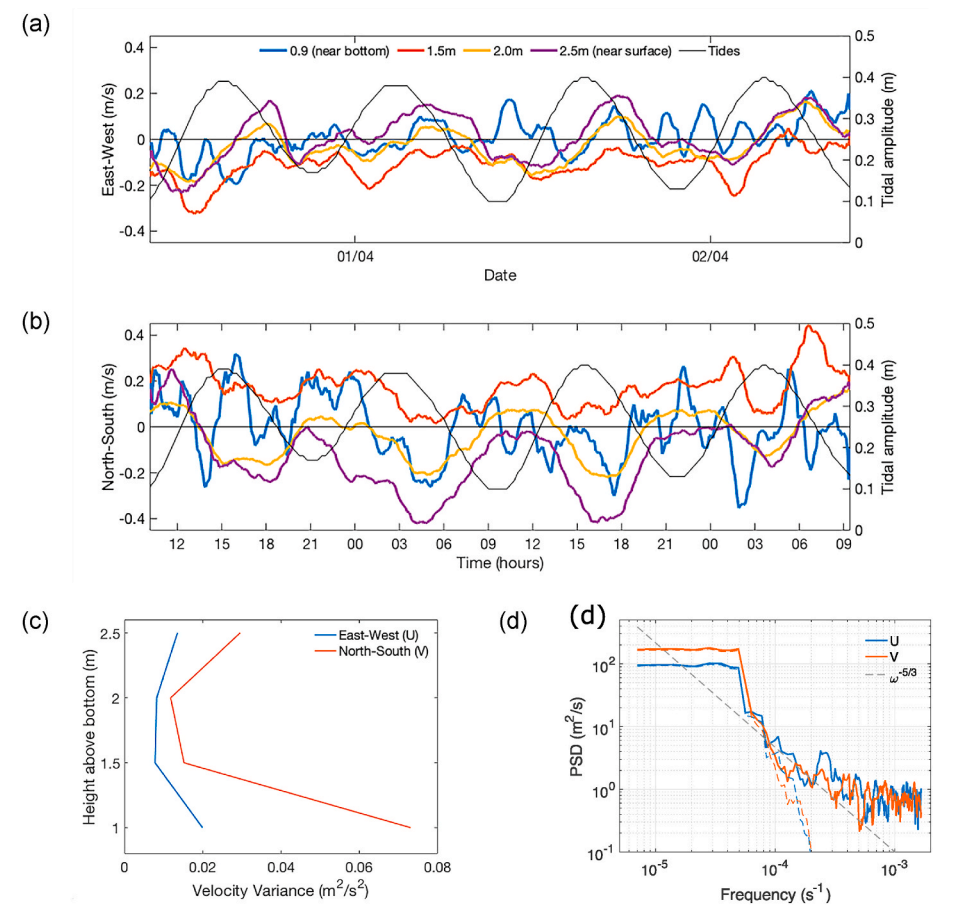


Fig. 3. (a, b) East-West (U) and North-South (V) velocities at different depths near Dry Bar, calculated from ADCP data, with a 30 min running mean filter applied. The height above the bottom is noted in the legend. (c) Velocity variance as a function of height above bottom (distance from AWAC + 0.1 m). (d) Frequency spectrum of the U and V velocity at height of 2.0 m. Red and blue dashed lines show the power spectrum of the smoothed velocity time-series shown in panels a and b; the dashed gray line marks the -5/3 power law. The behavior was qualitatively similar at 1.5 m and 2.5 m. (For interpretation of the references to color in this figure legend, the reader is referred to the Web version of this article.)

was preferentially towards the north-north-west, with signs of a strong south-south-east return flow at heights of 2.0 and 2.5 m. This slight preference for north-south flow may be a result of bottom topography, which has contours running north-south near this location, orienting the flow in the same direction.

The velocity variance generally decreases with depth/increases towards the surface (Fig. 3c). The variance of flow increased slightly in the bottom bin, due to the generation of turbulence in the bottom boundary layer. Variance in the north-south motions was stronger than east-west motions, likely a sign of topographic orientation of the flow.

In the frequency power spectrum of the currents (Fig. 3d), tidal motions dominated with time scales longer than approximately 6–7 h (frequency: $5\times 10^{-5}~\text{s}^{-1}$). There is a steep drop in power at periods around 4–6 h, followed by a semblance of a -5/3 power law at periods in the range of ~ 1 –4 h (8 $\times 10^{-5}~\text{s}^{-1}$ to 3 $\times 10^{-4}~\text{s}^{-1}$). This steep drop off supports that the slower motions, tidal and low-mode wind driven, are significantly dominant (at least 1 order of magnitude in power) over processes that might be generating motions at faster time scales, such as waves, hydraulic bores, 3D turbulence, etc. This is at least true at 2.0 m (shown here) and 2.5 m (not shown); the drop off was less steep at 1.5 m (not shown).

The -5/3 power law behavior is the same as what would be expected for 3D turbulence, but occurs at periods that are physically too long for 3D turbulence to be playing a role. This power law behavior is probably indicative of internal waves riding the stratification in the bay, which do produce qualitatively similar spectral slopes in the deep ocean (Garrett and Munk, 1972). At the highest resolved frequencies, or periods <0.5-1 h, the spectrum flattens out, indicating that the noise floor of the instrument as configured has been reached. A time of 0.5 h (30 min) was hence used to smooth (moving average) the time-series and obtain the dominant signal with minimal influence from noise for visualization.

The spectra for the smoothed signal in Fig. 3a–b, is shown as dashed lines in Fig. 3d, demonstrating that the smoothed (low-pass) signal is primarily composed of the strong flows associated with tides and slow persistent flows generated by the winds.

3.3. Drifters

3.3.1. Flow patterns

The drifter tracks revealed large-scale circulation patterns during the time of the experiment (Fig. 4). On Days 1–3, the drifters moved to the east, then on Day 4, they drifted northwestward, towards Indian Pass, with velocities ranged from 0.03 to 0.6 m s $^{-1}$. The smooth nature of the drifter trajectories suggested that most of the kinetic energy was in the longer spatial scales, rather than small-scale flow features. This spatial smoothness is complementary to the Eulerian frequency spectra (Fig. 3d), which showed a sharp drop off in energy at time scales faster than 4–6 h. Similar to the frequency spectrum, this suggests that there are strong flows steered by bathymetry, which have a large spatial scale structure that is forced by winds and tides. Overlain are much weaker small-scale currents that are driven by wind driven waves, stratification, and bathymetric interactions.

3.3.2. Eddy diffusivities

We used the four drifter trajectories with the higher resolution GPS sensors to estimate eddy diffusivity using the autocorrelation of the residual velocity time series (details of the calculation are presented in Supplementary Material B and high-resolution trajectories are shown in Figure B1). Fig. 4 b,c shows the eddy diffusivity estimates as a function of the speed of the mean, or large-scale flow, and the residual or eddy speed. Here the mean was defined as a running average with half window width of 1 h, further discussion of this choice and plots of mean and

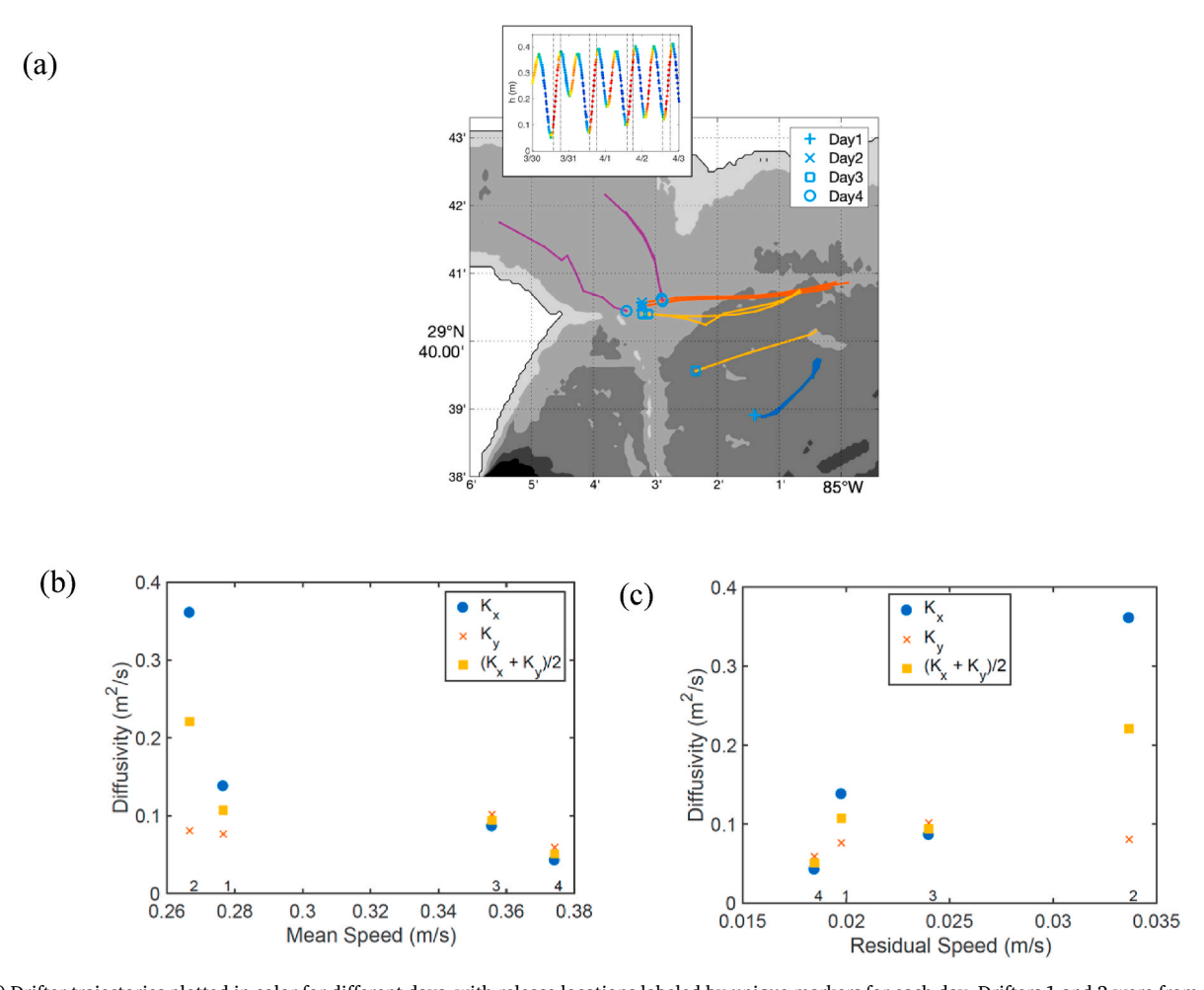


Fig. 4. (a) Drifter trajectories plotted in color for different days, with release locations labeled by unique markers for each day. Drifters 1 and 2 were from the sets of drifters on Days 2 and 3 that went to the east, and drifters 3 and 4 are the eastern pair of drifters released on Day 4 that went to the north (also see Figure B1). Bathymetric contours (1 m levels) are shown in gray shading. Inset plot depicts the tidal signal, with the duration of the float releases (always during the flood tide) marked by thin dashed vertical lines. (b, c) Drifter diffusivities from the GPS drifters, as a function of mean speed (b) and residual speed (c). The drifter number is indicated at the bottom of the plots for each data point. K_x and K_y are the diffusivities in the east-west and north-south directions. (For interpretation of the references to color in this figure legend, the reader is referred to the Web version of this article.)

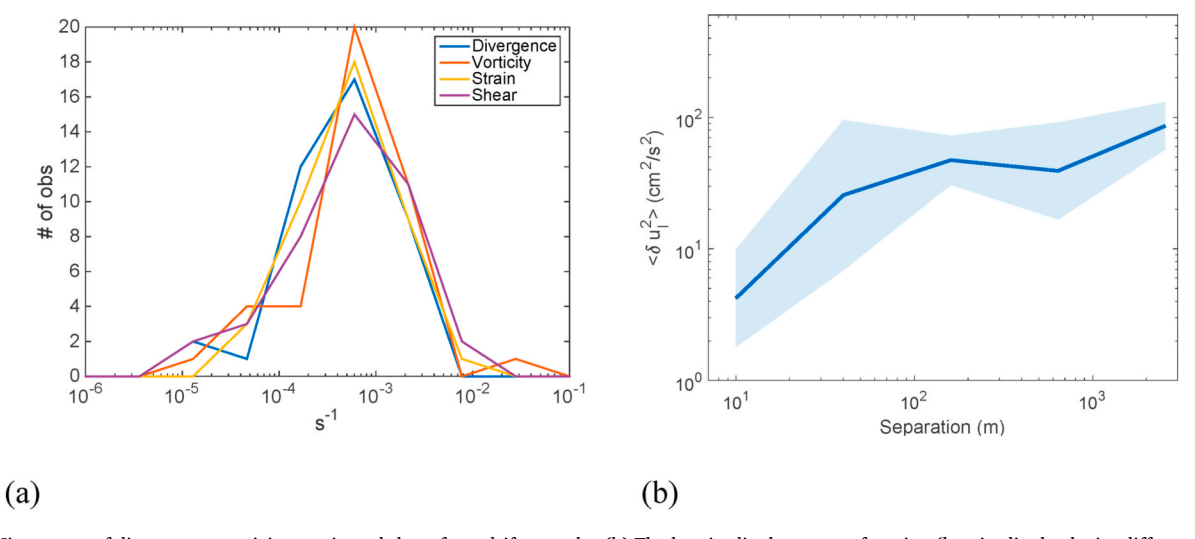


Fig. 5. (a) Histograms of divergence, vorticity, strain and shear from drifter tracks. (b) The longitudinal structure function (longitudinal velocity difference squared) as a function of separation distance.

residual velocity are in Supplementary Material B. The characteristic magnitude of the eddy diffusivity was $0.1~{\rm m}^2~{\rm s}^{-1}$. While the data set is limited, there is some suggestion that the eddy diffusivity increased with increasing eddy speeds and decreased with increasing mean flow speeds. Two of the four drifters (drifters 1 and 2), which traversed from west to east, show an enhanced zonal diffusivity in the direction corresponding to the mean flow, suggesting the influence of shear flow on dispersion. Drifters 3 and 4 show isotropic diffusivity, not enhanced in any particular direction. For these two drifters the two components of diffusivities remain isotropic, even if the diffusivities are decomposed in along and across mean flow directions (not shown).

3.3.3. Kinematics

As the drifters were released in triplets, we were able to use a least squares approach to estimate the local velocity gradients, and estimate the shear, strain, vorticity and divergence (method described in Supplementary Material C). Histograms of these quantities are shown in Fig. 5a and are quite similar. A median value of $5\times 10^{-4}~\text{s}^{-1}$ was observed, indicating that the Rossby number (vorticity/f) in the bay is larger than 1 and the flow is not dominated by rotation as is the case in the open ocean. However, the magnitudes of these gradients suggest that the velocity gradients in the bay are not very strong relative to the size of the bay. For a sinusoidal spatial distribution, a velocity scale of $0.2~\text{m s}^{-1}$ and a gradient of $5\times 10^{-4}~\text{s}^{-1}$ (median of the histogram) implies a wavelength of almost 2 km, which is about a quarter of the bay width. This scale is close to that of the peak in the energy spectra.

The longitudinal second order velocity structure function, which quantifies the velocity that stretches fluid particles apart, is shown in Fig. 5b. As there were very few drifter deployments, $S2_l$ is quite noisy but shows a modest increase as the separation distance increases. This suggests that the drifters were being separated at an approximate velocity of 2 cm s⁻¹ at separations of 10 m, and 10 cm s⁻¹ at separations of 500 m-1 km.

3.4. Dye transport

3.4.1. Patch

The first dye release (Patch 1) was initiated on Day 3 (April 1, 2015) in the immediate vicinity of a visible flotsam line associated with an incoming tidal front (Fig. 6a).

The surface salinity between opposite sides of the front differed by about 4. The water column was vertically stratified with a salinity

difference of 5 between surface (28) and bottom (33 at 1.7 m) (Fig. 6b). During the deployment, winds blew from the west at 5-6 m s⁻¹, and surface currents were oriented towards the southeast at 0.14 ± 0.06 m s $^{-1}$. Flow at 1.5 m above the bottom was preferentially towards the northnorthwest, with signs of a strong south-south-east return flow at 2.0 and 2.5 m from the bottom. This slight preference for north-south flow may be a result of bottom topography, which has contours running northsouth near this location, orienting the deeper flow in the same direction.

The dye was released at 08:18 EST. Eleven minutes after the release (08:29), the area of the dye patch measured approximately $380~\text{m}^2$. The patch was slightly elongated on its NNW – SSE axis, but it maintained a roughly ellipsoid shape throughout the experiment. The dye patch moved towards the east, and streaks of dye radiated away from the flotsam line (Fig. 6a, insets). The dye patch continued to spread to the east and developed a sharp boundary on the south-side of the patch along the flotsam line of the front.

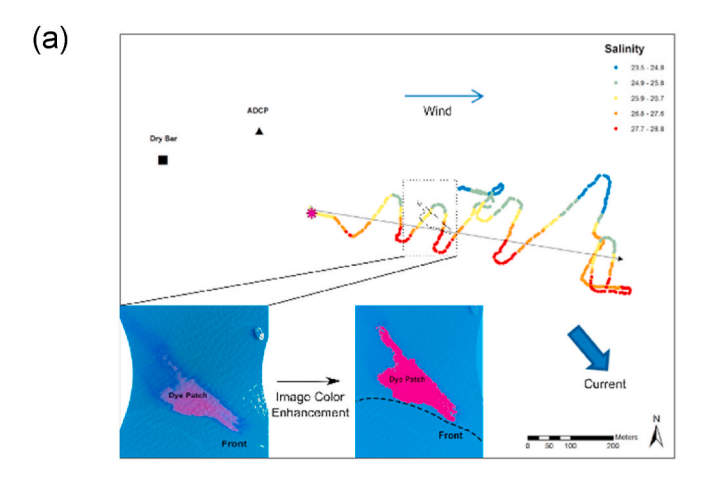
Around 17 min after dye release (08:35), the dye patch started to separate from the flotsam line, while remaining cohesive and parallel to it. By 08:49 the dye patch size had increased to an area of approximately 540 m², corresponding to a growth rate or diffusivity of 0.134 m² s $^{-1}$. Over the course of the next 20+ minutes, the patch continued to disperse and became less distinguishable. Drone photography ended 52 min after the dye release (09:10). Over the course of the observation, the dye patch moved $\sim\!\!770$ m to the east in 52 min, at an average speed of 0.3 \pm 0.1 m s $^{-1}$ (n = 7).

3.4.2. Patch 2

The second dye release (Patch 2) started at 10:29 EST on Day 4 under relatively calm conditions with wind from the ESE at 2-3 m s⁻¹. The water column was highly stratified – surface salinity was 10 and bottom (2.0 m) salinity was 32 (Fig. 6b).

The AWAC was retrieved an hour before the Day 4 dye release; however, 1–2 h before the dye release surface currents were flowing towards the N – NNW at 0.17 \pm 0.06 m s $^{-1}$ (range: 0.07–0.24 m s $^{-1}$). Immediately after the dye release (10:33), the area of the dye patch measured 78 m 2 . The patch developed an ellipsoid shape with a major axis (30 m long) oriented northwest to southeast (minor axis 6 m) (Fig. 7a–c).

The patch began to stretch along that same axis leading to an elongated shape with a dense kernel of dye at the northwest patch edge and a much larger but less dense filament towards the southeast. Over the next 15 min, the dye patch continued to elongate as it was advected to the



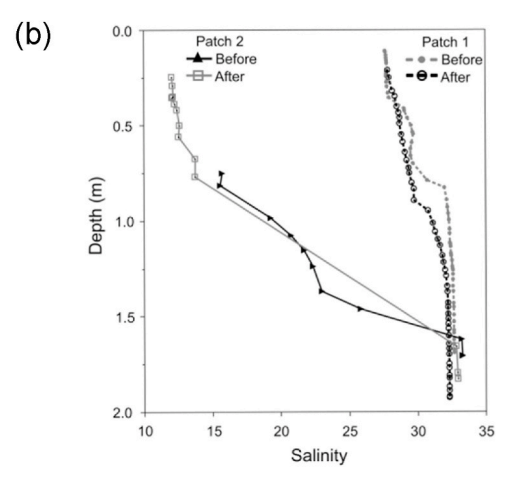
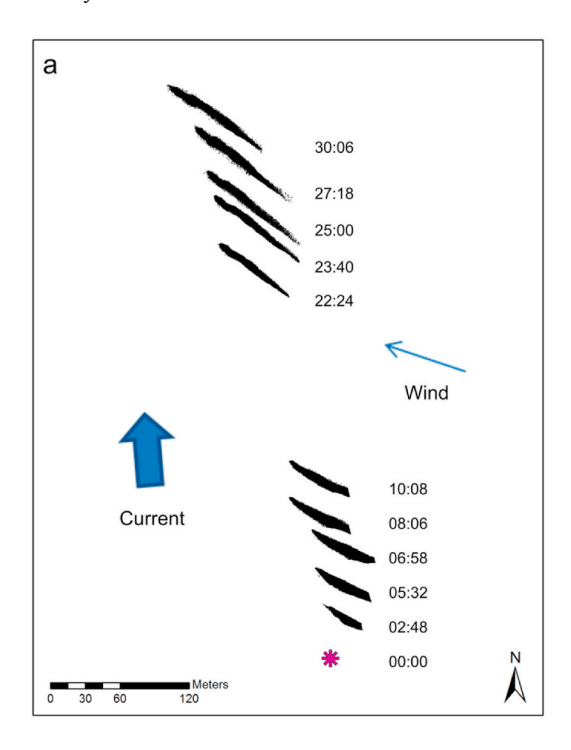


Fig. 6. (a) Map of dye release experiment 1. Pink asterisk: Patch 1 release location. Long black arrow: advection trajectory of the dye patch. Multicolored line: Salinity of water 0.5 m below the surface, with color representing salinities as listed in the upper right corner of the map. Data were collected with an onboard flow-through instrument and indicated the presence of a salinity front. Left inset: Example of drone imagery. Right inset: Same image after contrast enhancement; dashed line denotes the position of flotsam line (visible in left inset) along the density gradient. The current and its direction were calculated from the AWAC data (b) Vertical stratification of the water column immediately before dye release and after drone monitoring of the dye patch concluded. (For interpretation of the references to color in this figure legend, the reader is referred to the Web version of this article.)



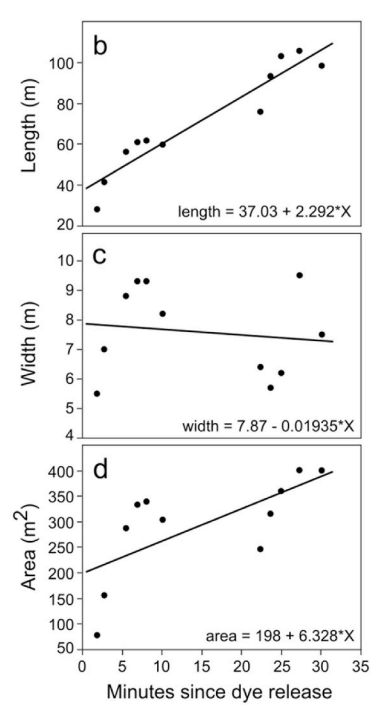


Fig. 7. (a) Map of Patch 2 advection and dispersion. The dye was released at the location of the pink asterisk and tracked to the NNW for 31 min. Black shapes represent the shape and location of the dye patch at the indicated time (minutes: seconds) after the release. The gap in the middle of the time series was when the drone battery was changed. The first five patch images had a small amount of the dye 'tail' cut off by the edge of the picture. Graphs b, c, and d show changes in the patch dimensions over time. Changes in (b) length (p < 0.0001, $R^2 = 0.9$), (c) width (p = 0.6, $R^2 = 0.02$), and (d) area (p = 0.02, $R^2 = 0.47$). (For interpretation of the references to color in this figure legend, the reader is referred to the Web version of this article.)

NNW, while its visible width decreased (Fig. 7b–c). The dye patch area initially grew linearly at a rate (diffusivity) of 0.71 m² s $^{-1}$ (43 m² min $^{-1}$) (Fig. 7d). Drone photography continued for 31 min and ended at 11:00 EST when the dye patch became visibly poorly defined. This dye patch moved $\sim\!500$ m to the NNW in 31 min, at an average speed of 0.3 \pm 0.1 m s $^{-1}$ (n = 10).

4. Discussion

Our study demonstrates how hydrodynamics can control small-scale tracer distribution in AB and provides insights on how these physical processes may influence phytoplankton patch characteristics in shallow estuarine environments. Divergence, diffusivity, vorticity, shear and strain rates produced from our measurements can be implemented in ecological models of AB phytoplankton development and help us understand and quantify primary production in this estuary. Likewise, these rates can be applied to estuaries with similar environmental settings (e.g., the numerous northern Gulf estuaries) facilitating improved estimates of the contribution of these estuaries to the productivity of the Gulf, which affects its fisheries, oxygen dynamics and local economies.

4.1. Effect of flow properties on patchiness

By definition, plankton cannot move against water flow, and the influence of complex estuarine current settings on phytoplankton distribution thus can be investigated with drifter and dye deployments. The drifters simultaneously traced the currents at multiple locations within AB and revealed how the flow can affect phytoplankton patchiness by stirring or stretching fluid parcels apart. The drifter trajectories and velocity frequency spectra from the AWAC suggest that flow in AB can be decomposed into a large-scale component driven by tides and winds, superimposed by small scale flow variability resulting from density fronts, surface and internal waves, 3D turbulence, bathymetry and coastlines. Ensuing stirring rates, determined from horizontal shear and strain rates, were on the order of $10^{-4} - 10^{-3} \, \mathrm{s}^{-1}$, or 2–3 orders of magnitude greater than typical open ocean strain rates ($10^{-6} \, \mathrm{s}^{-1}$, e.g., Martin, 2003; Sundermeyer and Ledwell, 2001). This substantially enhanced stirring underlines the difference between the estuarine and

ocean settings critical for phytoplankton patch dynamics. The stretching rates ranged from 2 to 10 cm $\rm s^{-1}$ at scales of 10–1000 m, which can potentially separate two fluid parcels over the entire width of AB in a single tidal cycle.

The diffusivity estimates from the drifters and dye ranged from 0.1 to 0.4 m 2 s $^{-1}$ and 0.1–0.7 m 2 s $^{-1}$, respectively, corresponding to length scales of a few 100s of meters (dye patch size) and time scales shorter than about an hour (following the definition of the mean path for the drifters). The agreement of the values obtained with the two independent methods strengthens and confines the calculated diffusivity. Bogucki et al. (2005) estimated a similar horizontal diffusivity of 0.1 m 2 s $^{-1}$ on scales of 10 m from aerial imagery of dye dispersion in an embayment. Our estimates are also broadly consistent with the diffusivity compilation in Okubo (1971), but smaller than canonical estimates from coastal (Rypina et al., 2016) and open ocean regions (Balwada et al., 2016), for which larger values can be expected.

Despite the rapid stretching rates indicated by the strain field, the concentration anomalies associated with small-scale fronts of environmental tracers (salinity and chlorophyll) were relatively small compared to the gradients associated with large scale filaments and gradients that develop as water mixes from the river, East Bay, and the Gulf of Mexico. This is complementary to the results of Geyer et al. (2018), who found that the small chlorophyll filaments correspond to about 10% of the biomass in the bay. This relatively small variability at small scales may be explained by the rapid flushing times of the bay (6–12 d); i.e., the larger filaments are flushed out of the bay before they can break into smaller filaments. High-resolution modeling studies of the bay or a study that follows chlorophyll filaments over a longer time period would be of value to test the validity of this hypothesis.

4.2. Physical dispersal revealed by dye patch evolution

In the typically turbid estuarine waters where light may penetrate only a couple of meters, the surface water layer is central for phytoplankton development, and our aerial imagery of dye patch development provided insights into physical processes that can control plankton distribution and dispersal (Bogucki et al., 2005; Clark et al., 2014). While the dye images provide limited information on the vertical

distribution of the dye (~ upper 10 cm), they allow the exploration of lateral transport, stirring and diffusivities. Patch 1 demonstrated how two physical processes affect patch evolution in the shallow estuarine environment in opposite ways: shear – causing gradients in transport – produced filaments and diffuse patch boundaries, while density fronts – limiting transport in across-front direction – caused sharp patch boundaries (Fig. 6a). The combination of these processes resulted in a patch with asymmetrical shape and concentration gradients, and can help explaining the asymmetrical Chl *a* peak that was observed in AB by Geyer et al. (2018) along the Apalachicola River plume front (Fig. 8).

Observations of such phytoplankton concentration gradients at fronts were explained with passive accumulation or enhanced growth stimulated by shear-induced nutrient fluxes (Franks, 1992; Largier, 1993; Dustan and Pinckney, 1989). Our dye experiment demonstrated that physical processes alone can produce these distribution patterns (Fig. 6a).

Patch splitting by vertical shear. Patch 1 moved in an ESE direction despite a general current flow towards the SE. This was caused by the westerly wind, moving the surface water layer in ESE direction and generating shear between surface and subsurface layers that led to the formation of dye tracer filaments at the northern trailing edge of the dye patch (Fig. 6a insets). This substantial vertical shear is also reflected in the AWAC velocity measurements (Fig. 2a–b). The feathering and filament formation seen on the photographs was partly caused by dyed subsurface water moving in the SE direction, separating from the ESE moving surface layer. Shear processes producing water layers moving in different directions thus can separate a well-confined phytoplankton patch into two patches, one in the surface layer, and the other in the subsurface layer. Such spreading due to vertical shear so far has not been addressed in AB models as these models so far simulated vertically integrated flow (e.g., Huang et al., 2002a; Huang et al., 2002b).

The evolution of Patch 2 underlines the role of wind-induced surface layer movement on patch development. In contrast to Patch 1, Patch 2 was influenced by wind and current moving in similar directions. The northward advection of Patch 2 by water currents was modulated by wind from the ESE such that the patch was stretched into a long ribbon shape (Fig. 7a). The leading northwest edge of the dye patch remained a more intense red, tracing the surface layer, which was pushed towards the WNW by the wind more quickly than the dye in the southeast 'tail' of

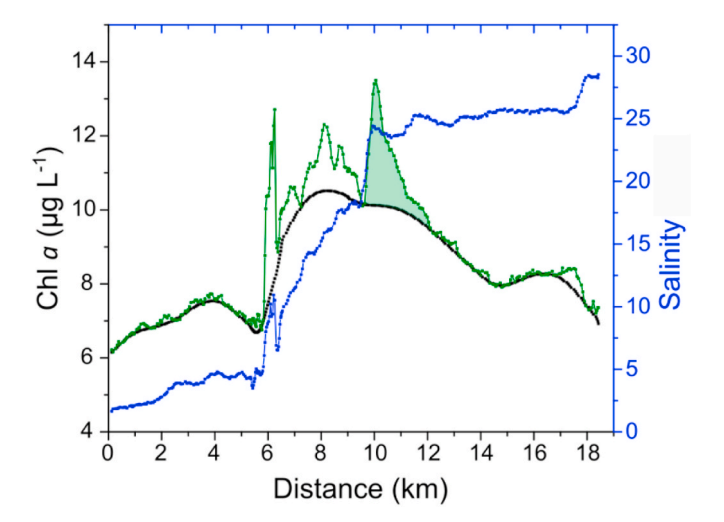


Fig. 8. Asymmetrical Chl a patch (green shaded area at distance 9.5–12 km) at a salinity front in AB. Chl a (green) and salinity (blue) were measured along a transect from the Up River site (0 km) to Dry Bar (19 km) (see Fig. 1a for station locations). The black baseline delineates large-scale Chl a distribution. These Dataflow measurements were conducted on August 29, 2011, within an associated research study reported by Geyer et al. (2018). (For interpretation of the references to color in this figure legend, the reader is referred to the Web version of this article.)

the patch that was entrained in slightly deeper water, again evidenced by the shift in color from red to blue.

Patch widths in straining flow. The stretching of Patch 2 by coherent wind and current movement led to a narrowing of the patch and the question arises whether this narrowing would continue and what ultimately the limitations of this process are. A minimum phytoplankton patch width has been theorized to exist for a patch filamented by a straining flow (Garrett, 1983; Martin, 2000; Sundermeyer and Price, 1998), and this width can be determined if the diffusivity and strain rate are known, such that

$$L = (K/\gamma)^{1/2},$$

where L is the minimum patch width, K is the horizontal eddy diffusivity, and γ is the mean strain rate of the flow. Using the minimum observed Chl a peak width of O(100 m) observed by Geyer et al. (2018) as the 'minimum' peak width and a strain rate on the order of 10^{-4} or O (10^{-4}) derived here, we can solve for the effective diffusivity, which is estimated as O(1 m² s⁻¹). This is slightly higher than K at a similar scale O(0.5 m² s⁻¹) calculated from the drifter dispersion and dye spreading, which is to be expected as the minimum widths observed by Geyer et al. (2018) may be limited by the sampling spatial resolution.

The phytoplankton population growth rate, μ_{net} , does not affect the minimum patch width, as long as $\mu_{\text{net}}/\gamma < 2.5,$ otherwise growth rates are expected to affect the steepness of the slope as it relates to diffusion and strain (Martin, 2000; McLeod et al., 2002). Growth rates in AB have been estimated as $\mu_{net} = 0.08-1.92~d^{-1}$ (Putland and Iverson, 2007), suggesting that growth does not have substantial effect on the slopes of the phytoplankton peaks in the straining flow we observed (all combinations of 0.08–1.92 $d^{-1}/10^{-3} - 10^{-4} s^{-1} < 2.5$). This is also in agreement with the spectral analysis of chlorophyll and salinity concentrations, showing that the spatial structures of these tracers are potentially steered by similar dynamics. For μ_{net}/γ to be greater than 2.5, μ_{net} would need to exceed 20 d⁻¹ to overcome strain rates of 10^{-4} s⁻¹. Whereas a phytoplankton community with $\mu_{net} = 1.92 \ d^{-1}$ divided by a smaller strain rate, such as that observed in the open ocean (10^{-6} s^{-1}) , would be expected to influence a patch's structure in a straining field $(1.92 \text{ d}^{-1}/10^{-6} \text{ s}^{-1} > 2.5)$. These values further emphasize the role of stirring on estuarine phytoplankton at these scales.

4.3. Effect of timescales

Most phytoplankton species' reproduction rates are on the scale of hours to days (Harris, 1986), indicating that dispersion at rates observed from our dye patch experiments are too fast for phytoplankton growth to cause patch formation at this scale. Therefore, estuarine phytoplankton patches O(10–100 m) are more likely to form when diffusivity is reduced (Koseff et al., 1993), through passive accumulation at features such as fronts (Largier, 1993), in still areas of the bay that are not rapidly flushed, or when larger patches are stretched or divided. Zooplankton grazing rates (0.07–1.94 d $^{-1}$) in AB can be similar to the phytoplankton growth rates (0.08–1.92 d $^{-1}$) (Putland and Iverson, 2007). To understand patch dynamics in estuaries, the effect of physical processes on both phytoplankton and zooplankton populations thus needs to be determined

5. Conclusions

Our process study, designed to contribute to a better understanding of the physical processes that influence spatial phytoplankton distribution, characterizes drivers of small-scale distribution patterns as observed in our example data collected in AB in 2011 and also estuarine phytoplankton distributions in general. Current measurements combined with dye patch and drifter behavior offered insights into the non-biological processes impacting short-term phytoplankton patch dynamics in estuarine settings. The results highlight differences between

controls of plankton patch development in shallow estuarine and deeper ocean settings. Dye patches were transported and dispersed within shorter time scales than phytoplankton reproduction rates; therefore, the formation and dispersion of estuarine phytoplankton patchiness at this spatial scale (1–100 m) are strongly governed by physical processes. A similar conclusion was also reached by comparing spatial variability in a passive tracer (salinity) and a biologically-active tracer (chlorophyll). The formation and dispersal of smaller-scale patches influences larger-scale spatial features (Levin, 1992; van Haren et al., 2004). Only through a better understanding of the spatial and temporal distribution of phytoplankton can we design measurement protocols that will allow producing realistic estimates of phytoplankton standing stock and biomass dynamics. This study provides new insights into processes that determine phytoplankton distribution in estuarine settings; however, the extent of the interactions between features at different spatial scales, such as those observed in Geyer et al. (2018) requires further investigation.

CRediT authorship contribution statement

Natalie L. Geyer: Conceptualization, Investigation, Data curation, Formal analysis, Visualization, Writing – original draft, Writing – review & editing, Funding acquisition, Supervision. Dhruv Balwada: Data curation, Writing – review & editing, Writing – original draft, Formal analysis, Conceptualization, Visualization, Software, Methodology, Investigation. Elizabeth Simons: Data curation, Formal analysis, Investigation, Writing – original draft, Writing – review & editing. Kevin Speer: Funding acquisition, Writing – review & editing, Investigation, Formal analysis, Data curation. Markus Huettel: Conceptualization, Data curation, Formal analysis, Investigation, Methodology, Project administration, Resources, Supervision, Writing – original draft, Writing – review & editing, Funding acquisition.

Declaration of competing interest

The authors declare that they have no known competing financial interests or personal relationships that could have appeared to influence the work reported in this paper.

Acknowledgements

We thank the Apalachicola National Estuarine Research Reserve (NERR) staff for providing boat time and assistance to conduct field work, Michael S. Wetz (TAMU-CC) for helpful discussions during planning, Tom Kelly and Christian Gredzens for assistance with image and spatial analysis of the drone pictures, and Xu Chen, Carlowen Smith, Jon Christophersen, Erick Olvera, and Tachanat Bhatrasataponkul for helping to finalize the project plan and collect field data. Funding for this research was provided by the National Oceanic and Atmospheric Administration NERR Graduate Research Fellowship (grant number NA11NOS4200083) to NLG and by the Florida State University. D.B. and K.S. acknowledge support from NSF OCE 1231803 and M.H. support from NSF OCE 1851290.

Appendix A. Supplementary data

Supplementary data to this article can be found online at https://doi.org/10.1016/j.ecss.2022.107811.

References

- Babiano, A., Basdevant, C., Le Roy, P., Sadourny, R., 1990. Relative dispersion in twodimensional turbulence. J. Fluid Mech. 214, 535–557.
- Bailey, T.E., 1966. Fluorescent-tracer studies of an estuary. Journal (Water Pollution Control Federation) 1986–2001.

- Balwada, D., Speer, K.G., LaCasce, J.H., Owens, W.B., Marshall, J., Ferrari, R., 2016. Circulation and stirring in the southeast pacific ocean and the scotia sea sectors of the antarctic circumpolar current. J. Phys. Oceanogr. 46, 2005–2027.
- Behrenfeld, M.J., Boss, E., Siegel, D.A., Shea, D.M., 2005. Carbon-based ocean productivity and phytoplankton physiology from space. Global Biogeochem. Cycles 19
- Behrenfeld, M.J., Falkowski, P.G., 1997. Photosynthetic rates derived from satellite-based chlorophyll concentration. Limnol. Oceanogr. 42, 1–20.
- Bogucki, D.J., Jones, B.H., Carr, M.-E., 2005. Remote measurements of horizontal eddy diffusivity. J. Atmos. Ocean. Technol. 22, 1373–1380.
- Boynton, W.R., Kemp, W.M., Keefe, C.W., 1982. A comparative analysis of nutrients and other factors influencing estuarine phytoplankton production. In: Victor, S.K.A.D. (Ed.), Estuarine Comparisons. Academic Press, New York, pp. 69–90.
- Bricker, S.B., Longstaf, B., Dennison, W., Jones, A., Boicourt, K., Wicks, C., Woerner, J., 2008. Effects of nutrient enrichment in the nation's estuaries: A decade of change. Harmful Algae 8, 21–32.
- Brouwer, R.L., de Schipper, M.A., Rynne, P.F., Graham, F.J., Reniers, A.J., MacMahan, J. H., 2016. Surfzone monitoring using rotary wing unmanned aerial vehicles. J. Atmos. Ocean. Technol. 32, 855–863.
- Bundy, M.M., 1992. Estuarine management from a global economic-perspective. Water Sci. Technol. 26, 2735–2739.
- Camargo, J.A., Alonso, A., 2006. Ecological and toxicological effects of inorganic nitrogen pollution in aquatic ecosystems: a global assessment. Environ. Int. 32, 831–849.
- Chant, R.J., Geyer, W.R., Houghton, R., Hunter, E., Lerczak, J., 2007. Estuarine boundary layer mixing processes: insights from dye experiments. J. Phys. Oceanogr. 37, 1859–1877.
- Clark, D.B., Lenain, L., Feddersen, F., Boss, E., Guza, R.T., 2014. Aerial imaging of fluorescent dye in the near shore. J. Atmos. Ocean. Technol. 31, 1410–1421.
- Cloern, J.E., Foster, S.Q., Kleckner, A.E., 2014. Phytoplankton primary production in the world's estuarine-coastal ecosystems. Biogeosciences 11, 2477–2501.
- Davis, R.E., 1991. Lagrangian ocean studies. Annu. Rev. Fluid Mech. 23, 43–64.Day, J.W., Kemp, W.M., Yáñez-Arancibia, A., Crump, B.C., 2012. Estuarine Ecology, second ed. ed. Wiley-Blackwell.
- DJI, 2017. Phantom 2 Vision+ specs (drone hardware and software information). htt ps://urldefense.com/v3/_https://www.dji.com/phantom-2-vision-plus.
- Dulaiova, H., Burnett, W.C., 2008. Evaluation of the flushing rates of Apalachicola Bay, Florida via natural geochemical tracers. Mar. Chem. 109, 395–408.
- Dustan, P., Pinckney, J.L., 1989. Tidally induced estuarine phytoplankton patchiness. Limnol. Oceanogr. 34, 410–419.
- Edmiston, H.L., 2008. A River Meets the Bay. A Characterization of the Apalachicola River and Bay System. Apalachicola National Estuarine Research Reserve. Florida Department of Environmental Protection, Apalachicola, p. 188.
- Fischer, H.B., 1976. Mixing and dispersion in estuaries. Annu. Rev. Fluid Mech. 8, 107–133.
- Franks, P.J., 1992. Phytoplankton blooms at fronts: patterns, scales, and physical forcing mechanisms. Rev. Aquat. Sci. 6, 121–137.
- Franks, P.J., 2005. Plankton patchiness, turbulent transport and spatial spectra. Mar. Ecol. Prog. Ser. 294, 295–309.
- Garrett, C., 1983. On the initial streakness of a dispersing tracer in two-and threedimensional turbulence. Dynam. Atmos. Oceans 7, 265–277.
- Garrett, C., Munk, W., 1972. Space-Time scales of internal waves. Geophys. Fluid Dynam.
 3, 225–264.
 Geyer, N.L., Huettel, M., Wetz, M.S., 2018. Phytoplankton spatial variability in the river-
- dominated estuary, Apalachicola bay, Florida. Estuar. Coast 41, 2024–2038. Geyer, W.R., Signell, R.P., 1992. A reassessment of the role of tidal dispersion in estuaries
- Geyer, W.R., Signell, R.P., 1992. A reassessment of the role of tidal dispersion in estuaries and bays. Estuaries 15, 97–108.
- Harris, G.P., 1986. Phytoplankton Ecology: Structure, Function and Fluctuation. Chapman and Hall, London.
- Haury, L., McGowan, J., Wiebe, P., 1978. Patterns and processes in the time-space scales of plankton distributions. In: Steele, J.H. (Ed.), Spatial Pattern in Plankton Communities. Plenum Press, New York, NY, pp. 277–327.
- Huang, W., Foo, S., 2002. Neural network modeling of salinity variation in Apalachicola River. Water Res. 36, 356–362.
- Huang, W., Jones, W.K., Wu, T.S., 2002a. Modelling wind effects on subtidal salinity in Apalachicola Bay, Florida. Estuar. Coast Shelf Sci. 55, 33–46.
- Huang, W., Sun, H., Nnaji, S., Jones, W.K., 2002b. Tidal hydrodynamics in a multipleinlet estuary: Apalachicola Bay, Florida. J. Coast Res. 18, 674–684.
- Jimenez, F., Rodriguez, J., Bautista, B., Rodriguez, V., 1987. Relations between chlorophyll, phytoplankton cell abundance and biovolume during a winter bloom in mediterranean coastal waters. J. Exp. Mar. Biol. Ecol. 105, 161–173.
- Koseff, J.R., Holen, J.K., Monismith, S.G., Cloern, J.E., 1993. Coupled effects of vertical mixing and benthic grazing on phytoplankton populations in shallow, turbid estuaries. J. Mar. Res. 51, 843–868.
- Largier, J.L., 1993. Estuarine fronts: how important are they? Estuaries 16, 1–11.Levin, S.A., 1992. The problem of pattern and scale in ecology: the Robert H. MacArthur award lecture. Ecology 73, 1943–1967.
- Longhurst, A., 1995. Seasonal cycles of pelagic production and consumption. Prog. Oceanogr. 36, 77–167.
- Lucas, L.V., Koseff, J.R., Cloern, J.E., Monismith, S.G., Thompson, J.K., 1999. Processes governing phytoplankton blooms in estuaries. I: the local production-loss balance. Mar. Ecol. Prog. Ser. 187, 1–15.
- Lumpkin, R., Özgökmen, T., Centurioni, L., 2017. Advances in the application of surface drifters. Ann. Rev. Mar. Sci 9, 59–81.
- Mackas, D.L., Denman, K.L., Abbott, M.R., 1985. Plankton patchiness: biology in the physical vernacular. Bull. Mar. Sci. 37, 652–674.

- Madden, C.J., Day, J.W., 1992. An instrument system for high-speed mapping of chlorophyll a and physico-chemical variables in surface waters. Estuaries 15, 421–427
- Mahadevan, A., 2016. The impact of submesoscale physics on primary productivity of plankton. Ann. Rev. Mar. Sci 8, 161–184.
- Mansur, A.V., Brondizio, E., Roy, S., Hetrick, S., Vogt, N.D., Newton, A., 2016. An assessment of urban vulnerability in the Amazon Delta and Estuary: a multi-criterion index of flood exposure, socio-economic conditions and infrastructure. Sustainability Science 11, 625–643.
- Martin, A., 2005. The kaleidoscope ocean. Phil. Trans. Roy. Soc. Lond.: Mathematical, Physical and Engineering Sciences 363, 2873–2890.
- Martin, A.P., 2000. On filament width in oceanic plankton distributions. J. Plankton Res. 22, 597–602.
- Martin, A.P., 2003. Phytoplankton patchiness: the role of lateral stirring and mixing. Prog. Oceanogr. 57, 125–174.
- McLeod, P., Martin, A.P., Richards, K.J., 2002. Minimum length scale for growth-limited oceanic plankton distributions. Ecol. Model. 158, 111–120.
- Mirfenderesk, H., Hughes, L., Tomlinson, R., 2007. Verification of a Three Dimensional Advection Dispersion Model Using Dye Release Experiment, 16th Australasian Fluid Mechanics Conference (AFMC). School of Engineering, The University of Queensland, pp. 233–240.
- Molinari, R., Kirwan Jr., A., 1975. Calculations of differential kinematic properties from Lagrangian observations in the western Caribbean Sea. J. Phys. Oceanogr. 5, 483–491.
- Morey, S.L., Dukhovskoy, D.S., 2012. Analysis methods for characterizing salinity variability from multivariate time series applied to the Apalachicola bay estuary. J. Atmos. Ocean. Technol. 29, 613–628.
- Mortazavi, B., Iverson, R.L., Landing, W.M., Lewis, F.G., Huang, W., 2000. Control of phytoplankton production and biomass in a river-dominated estuary: Apalachicola Bay, Florida, USA. Mar. Ecol. Prog. Ser. 198, 19–31.
- Mortenson, E., 2013. Physical description and analysis of the variability of salinity and oxygen in Apalachicola bay. In: Earth, Ocean, and Atmospheric Sciences. Florida State University, Tallahassee, p. 55.
- Okubo, A., 1971. Oceanic Diffusion Diagrams, Deep Sea Research and Oceanographic Abstracts. Elsevier, pp. 789–802.
- Okubo, A., 1978. Horizontal dispersion and critical scales for phytoplankton patches. In: Steele, J.H. (Ed.), Spatial Pattern in Plankton Communities. Plenum Press, New York, N.Y., pp. 21–42
- Pal, B.K., Murthy, R., Thomson, R.E., 1998. Lagrangian measurements in lake ontario. J. Great Lake. Res. 24, 681–697.

- Prairie, J.C., Franks, P.J.S., Jaffe, J.S., Doubell, M.J., Yamazaki, H., 2011. Physical and biological controls of vertical gradients in phytoplankton. Limnol. Oceanogr. Fluid. Environ. 1, 75–90.
- Putland, J.N., Iverson, R.L., 2007. Microzooplankton: major herbivores in an estuarine planktonic food web. Mar. Ecol. Prog. Ser. 345, 63–73.
- Rabalais, N.N., Turner, R.E., Diaz, R.J., Justic, D., 2009. Global change and eutrophication of coastal waters. ICES J. Mar. Sci. 66, 1528–1537.
- Rabouille, C., Mackenzie, F.T., Ver, L.M., 2001. Influence of the human perturbation on carbon, nitrogen, and oxygen biogeochemical cycles in the global coastal ocean. Geochem. Cosmochim. Acta 65, 3615–3641.
- Roman, M., Zhang, X., McGilliard, C., Boicourt, W., 2005. Seasonal and annual variability in the spatial patterns of plankton biomass in Chesapeake Bay. Limnol. Oceanogr. 50, 480–492.
- Rypina, I.I., Kirincich, A., Lentz, S., Sundermeyer, M., 2016. Investigating the eddy diffusivity concept in the coastal ocean. J. Phys. Oceanogr. 46, 2201–2218.
- Smart, P., Laidlaw, I., 1977. An evaluation of some fluorescent dyes for water tracing. Water Resour. Res. 13, 15–33.
- Suara, K., Brown, R., Borgas, M., 2016. Eddy diffusivity: a single dispersion analysis of high resolution drifters in a tidal shallow estuary. Environ. Fluid Mech. 16, 923–943.
- Suijlen, J., Buyse, J., 1994. Potentials of photolytic rhodamine WT as a large-scale water tracer assessed in a long-term experiment in the Loosdrecht lakes. Limnol. Oceanogr. 39, 1411–1423.
- Sundermeyer, M.A., Ledwell, J.R., 2001. Lateral dispersion over the continental shelf: analysis of dye release experiments. J. Geophys. Res.: Oceans 106, 9603–9621.
- Sundermeyer, M.A., Ledwell, J.R., Oakey, N.S., Greenan, B.J.W., 2005. Stirring by small-scale vortices caused by patchy mixing. J. Phys. Oceanogr. 35, 1245–1262.
- Sundermeyer, M.A., Price, J.F., 1998. Lateral mixing and the north atlantic tracer release experiment: observations and numerical simulations of Lagrangian particles and a passive tracer. J. Geophys. Res. 103 (21), 481-421,497.
- Tauro, F., 2016. Particle tracers and image analysis for surface flow observations. Wiley Interdisciplinary Reviews: Water 3, 25–39.
- van Haren, H., Laurent, L.S., Marshall, D., 2004. Small and mesoscale processes and their impact on the large scale: an introduction. Deep Sea Res. Part II Top. Stud. Oceanogr. 51, 2883–2887.
- Watson, A.J., Ledwell, J.R., 2000. Oceanographic tracer release experiments using sulphur hexafluoride. J. Geophys. Res.: Oceans 105, 14325–14337.
- Wetz, M.S., Hutchinson, E.A., Lunetta, R.S., Paerl, H.W., Christopher Taylor, J., 2011. Severe droughts reduce estuarine primary productivity with cascading effects on higher trophic levels. Limnol. Oceanogr. 56, 627–638.
- Yu, Y., Zhang, H., Spencer, D., Dunn, R.J., Lemckert, C., 2016. An investigation of dispersion characteristics in shallow coastal waters. Estuar. Coast Shelf Sci. 180, 21–32